

In-Canopy Chemistry, Emissions, Deposition, and Surface Reactivity Compete to Drive Bidirectional Forest-Atmosphere Exchange of VOC Oxidation Products

Michael F. Link, Matson A. Pothier, Michael P. Vermeuel, Mj Riches, Dylan B. Millet, and Delphine K. Farmer*



Cite This: <https://doi.org/10.1021/acsestair.3c00074>



Read Online

ACCESS |

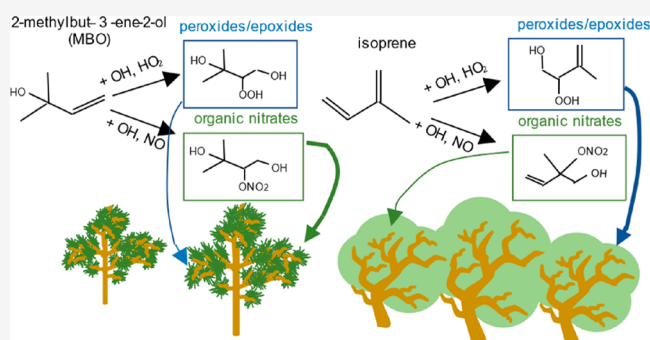
Metrics & More

Article Recommendations

Supporting Information

ABSTRACT: Dry deposition is an important sink of oxygenated volatile organic compounds (OVOCs) in forest ecosystems. In the summer of 2021, we measured concentration gradients and exchange velocities of oxidation products of isoprene and 3-methyl-3-buten-2-ol (MBO) from a Colorado Ponderosa pine forest as part of the Flux Closure Study (FluCS). MBO oxidation products exhibited bidirectional exchange over the forest. Vertical gradients of MBO oxidation products reveal in-canopy chemical production as a daytime source, whereas air transported from the urban outflow of the front range creates periods of enhanced deposition. Differences between our observed deposition velocities over the arid, sparse pine forest and those from a previous study over a temperate, dense mixed forest suggest that ecosystem type may impact deposition rates in ways not currently captured by GEOS-Chem. We show that a previously inferred increased OVOC solubility threshold on leaf cuticles is not likely to explain the observed rapid rates of deposition but instead suggest that peroxides/epoxides could undergo reactive uptake to broadleaf vegetation while organic nitrates could undergo reactive uptake to pine needles. We point to the need to understand the role of reactive OVOC uptake and its potential implications for bidirectional ecosystem-atmosphere exchange.

KEYWORDS: biosphere-atmosphere exchange, dry deposition, biogenic VOCs, eddy-covariance flux, organic nitrates, organic peroxides



INTRODUCTION

Forests simultaneously act as both sources and sinks of volatile organic compounds (VOCs) and ultimately serve as a major source of atmospheric reactive carbon.^{1,2} In the early stages of chemical transformation, VOCs react with oxidants (e.g., hydroxyl radical, OH) to form peroxy radicals (RO₂) that can then react with hydroperoxyl radicals (HO₂), nitrogen oxides (NO and NO₂), or other RO₂ to yield multifunctional oxidized VOCs (OVOCs). These OVOCs often contain peroxide, carbonyl, or nitrate moieties, which can make the molecules water-soluble and semivolatile in nature.³ Ultimately, forests mediate processes that drive air pollution including ozone production, aerosol formation, and atmospheric acidity through the exchange of OVOCs between the terrestrial ecosystem and the atmosphere.

While oxidation chemistry is a major source of many OVOCs originating from forests, dry deposition can be an important sink.⁴ Early investigations into forest-atmosphere exchange focused on relatively volatile molecules—like monoterpenes, isoprene, small alcohols, aldehydes, and ketones—that can be measured with proton-transfer reaction mass spectrometers.^{5–7} Other studies focused on organic

nitrates like peroxyacyl and alkyl nitrates.^{8,9} Recently, several studies have examined the role of dry deposition in controlling the flux of formic acid from forests.^{10–13} Among the population of OVOCs studied to date, few measurements of speciated early-generation OVOC fluxes exist to understand the magnitude of their dry deposition sink. Nguyen et al. (2015) found that the dry deposition lifetimes of several OVOCs originating from isoprene oxidation were comparable to their reactive lifetimes. The deposition measurements of Nguyen et al. (2015) have been used as the benchmark for OVOC deposition in several modeling studies that constrained in-canopy aerosol formation,¹⁴ organic nitrate hydrolysis rates,¹⁵ and global oxidant production and recycling from isoprene oxidation.¹⁶ However, different populations of OVOCs are present over different forest ecosystems due to

Received: November 2, 2023

Revised: February 28, 2024

Accepted: February 29, 2024

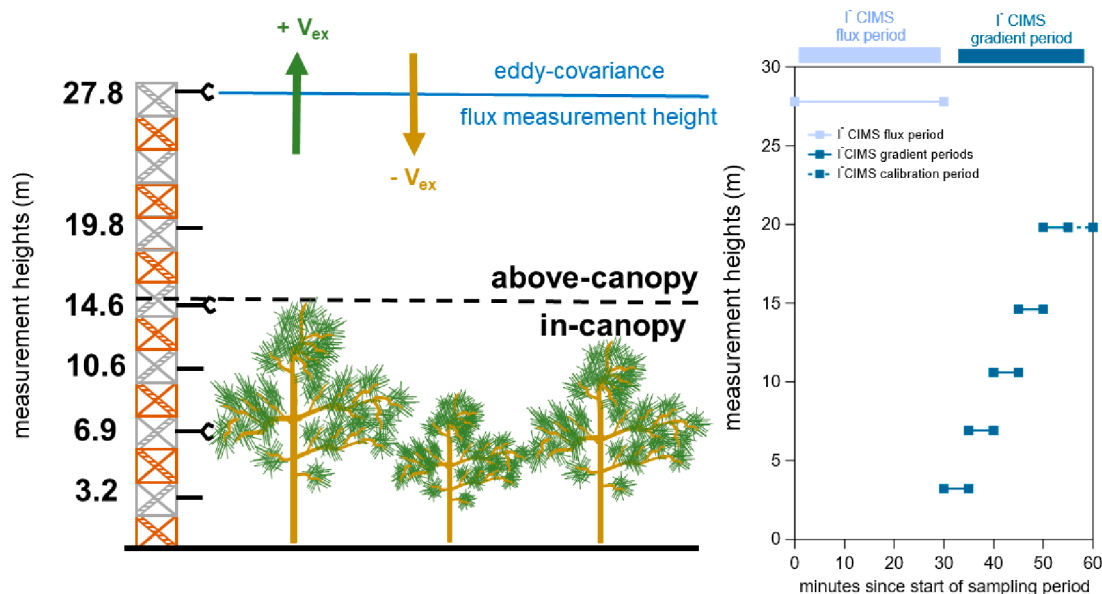


Figure 1. Measurement tower at the MEFO stands 30 m tall. The top of the forest canopy is approximately 15 m above ground level. For vertical gradient measurements, three inlets are sampled from within the canopy, and two inlets are sampled above the canopy. The I⁻ CIMS sampled from the flux line for the first half of every hour and from the vertical gradient system for the second half of every hour. Turbulence measurements were obtained by sonic anemometry at the three heights indicated in the diagram on the left.

varying precursor speciation,¹⁷ resulting in diverse chemical properties of volatility, reactivity, and solubility for the resulting OVOCs. Further, the physical structure of forest ecosystems varies substantially, resulting in differences not only across leaf area but also across soil and leaf properties. These differences in ecosystem structure impact the underlying mechanisms of dry deposition of particles,¹⁸ and we hypothesize that rates of OVOC deposition could also vary significantly across different forest ecosystems.

Our ability to describe and model chemical mechanisms has become more sophisticated over the past decade, and chemical transport models are better able to predict oxidation product concentrations.^{16,19} However, questions persist regarding the physical and chemical processes that regulate OVOC exchange between the forest and atmosphere.²⁰ Competing physical and chemical processes that induce biosphere-atmosphere exchange of OVOCs include dry deposition, direct plant emission, in-canopy reactive chemistry,^{12,21} and heterogeneous or multiphase reactions on the surfaces of leaves,²² water droplets,²³ and other ecosystem surfaces.²⁴ The result of these competing processes is that many OVOCs show bidirectional exchange.^{2,25} This bidirectional exchange influences the fate of OVOCs and ultimately how they impact the production of aerosol⁴ and the budgets of oxidants and NO_x.^{14,15,26} While canopy-resolved models have provided insight on in-canopy ozone fluxes,²⁷ few studies have investigated the in-canopy processes regulating the flux of key reactive OVOCs that contribute to oxidant flux and are produced from oxidation of major precursors, such as isoprene or 3-methyl-3-buten-2-ol (MBO). While isoprene has major biogenic emission sources from broadleaf vegetation and grasses²⁸ with broad geographical significance, MBO is primarily emitted from coniferous vegetation like Ponderosa or Scots pine with regional significance as a reactive atmospheric VOC in parts of western North America.²⁹ Thus, there is a clear need to understand the underlying processes controlling the forest-atmosphere exchange of biogenic oxidized organic compounds

in order to improve our capacity to model their sources²² and sinks—and thus atmospheric lifetimes and impacts.³⁰

Here, we present measurements of concentrations, fluxes, and vertical gradients of OVOCs collected at a Ponderosa pine forest. These measurements constrain the mechanisms driving bidirectional fluxes that determine the dry deposition velocities for a subset of biogenic OVOCs.

METHODS

Site and Sampling Description. The Flux Closure Study (FluCS) was held at the Manitou Experimental Forest Observatory (MEFO)³¹ in the summer of 2021 to study the biosphere-atmosphere exchange of VOCs within and above a Ponderosa pine forest. The site is comprised of relatively sparse (Photo S1) Ponderosa pine (median tree age of 61.5 years)³¹ new-growth with an understory dominated by grasses and shrubs. MEFO is located west of Colorado Springs in a subalpine, semiarid climate. Branch enclosure measurements revealed direct emissions of MBO and monoterpenes for Ponderosa pine.³² In contrast, isoprene and sesquiterpenes are emitted from the understory.³³

Gas-phase measurements of OVOCs were collected using an inlet system, installed along a 30 m tall tower, designed for the measurement of VOC fluxes using the flux-gradient approach and eddy-covariance methods.^{2,13,31} Two independent manifolds alternately sampled forest air from an eddy-covariance flux measurement line and a vertical gradient measurement system (Figure 1).

The two independent sampling systems were used to measure gradients and fluxes with two mass spectrometers, an iodide chemical ionization mass spectrometer (I⁻ CIMS; HR-ToF-MS, Aerodyne Inc.) and a proton-transfer-reaction mass spectrometer (PTR-MS; PTR-QiToF Ionicon Analytik). A complete description of the PTR-MS instrument configuration is presented in Vermeuel et al. (2023).³³ The two mass spectrometers alternated inlet systems (Figure S1). Each instrument spent 30 minutes sequentially sampling the

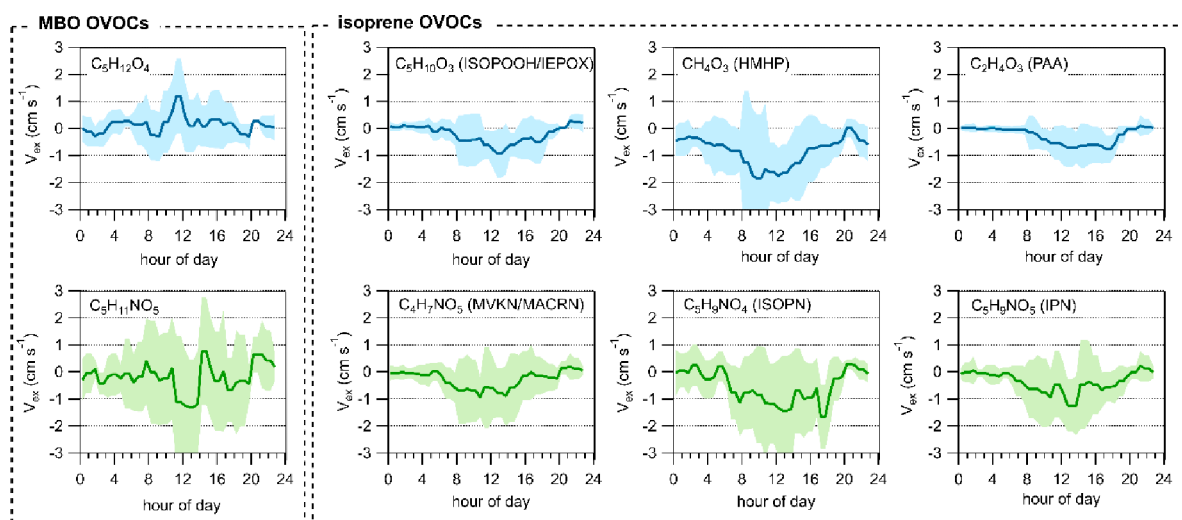


Figure 2. V_{ex} for peroxide/epoxide (top) and organic nitrate (bottom) OVOCs. The OVOCs within the dashed box to the left originate from MBO oxidation, and those in the box to the right originate from isoprene oxidation. Blue and green lines show diel half hour averages from the 16th to 22nd and 26th to 31st of August 2021, and shaded regions show the standard deviation.

gradient system followed by 30 continuous minutes on the flux line. The gradient system used a Teflon valve manifold to cycle between five identical sampling lines installed between 3 m and 28 m for 5 minutes each. Hourly calibrations occurred during the last 5 minutes of the 30 minute gradient sampling period. The flux line inlet was installed directly below a sonic anemometer mounted at 27.8 m on the tower.

All sampling lines were constructed from PFA tubing (1/2'' outer diameter, 30 m length) and continuously heated to 50 °C to minimize wall losses. Air was pulled through the gradient lines at 25 L per minute (lpm) and the flux line at 35 lpm. These different flow rates caused slightly different line-losses for some OVOCs and hindered direct comparison of concentrations for those species between the gradient and eddy-flux systems. However, the exchange velocities determined using the flux line are corrected for tubing effects (see below) and are independent of concentration. The vertical gradient system employed identical sampling lines for each height to avoid any line loss differences between them. As a result, the measured exchange velocities can be directly compared and interpreted against the measured vertical gradients.

I⁻ CIMS Measurements. I⁻ CIMS spectra were collected at 5 Hz and averaged to 10 s for gradient-resolved analyses. Hourly background subtraction was performed by sampling ultrahigh purity nitrogen. Instrument performance was evaluated using hourly three-point calibrations of C1 through C5 alkanolic acids. We mitigate the well-documented effects of ambient humidity on instrument sensitivity by introducing a flow of water vapor-saturated nitrogen into the ion-molecule reactor ($P_{\text{H}_2\text{O in IMR}} = 0.8$ mbar). The ion-molecule reactor temperature varied by ± 2 °C. Commercially available standards do not exist for the OVOCs at the center of this study, and synthesis and calibration of authentic standards are challenging. We present I⁻ CIMS data as mixing ratios estimated by a voltage scanning procedure described in Vermeuel et al. (2023), except for formic acid which we directly calibrated in the field using a permeation tube. We note that the mixing ratios and fluxes estimated for individual species from voltage scanning can carry order-of-magnitude

systematic uncertainties,³⁴ but these uncertainties do not impact the V_{ex} reported herein.

For eddy covariance analysis, we apply standard quality control filters for stationarity and turbulence as described in Vermeuel et al. (2023). The compounds measured by the I⁻ CIMS experienced considerable gas-wall equilibration times with both the sample tubing and the walls of the ion-molecule reactor (Figure S8). We correct for high frequency attenuation through the flux line using the empirical model of Horst (1997)³⁵ and by applying a flux attenuation factor³⁶ to exchange velocities for compounds measured by the I⁻ CIMS. Example lag-covariance and cospectra are presented in the Supporting Information (Figures S10 and S11), and we point the reader to Vermeuel et al. (2023) for a detailed presentation of flux quality control analyses that support the measurements in this manuscript. The Supporting Information contains additional information on data processing, instrument operation, and calibration procedures.

GEOS-Chem Modeling. We performed three model simulations over two forested domains using GEOS-Chem v13.3.0 (<http://geos-chem.org/>) with a full-chemistry mechanism to test our current understanding of terrestrial OVOC deposition. Dry deposition in GEOS-Chem is calculated using the Wesely (2007)³⁷ resistance model adapted to a global scale³⁸ with modifications for canopy radiative transfer³⁹ and observed OVOC uptake.⁴⁰ Model land cover is driven by leaf area index (LAI) derived from the Moderate Resolution Imaging Spectroradiometer (MODIS)⁴¹ and the Olson (2001)⁴² land maps from which 11 depositional land types are used.

The first model run uses GEOS-FP (Goddard Earth Observation System Forward Processing product) assimilated meteorology for a nested simulation at $0.25^\circ \times 0.3125^\circ$ from July 6th to October 1st, 2021, over a custom domain surrounding the MEFO ($\pm 3^\circ$ latitude and longitude). Details of this configuration can be found in Vermeuel et al. (2023), including one relevant update that scales the LAI in the MEFO-containing model grid cell to match the observed measurement footprint.³³ The second model run is configured identically to the first except that it has a spatial domain of $0.5^\circ \times 0.625^\circ$ and uses the Modern-Era Retrospective analysis for

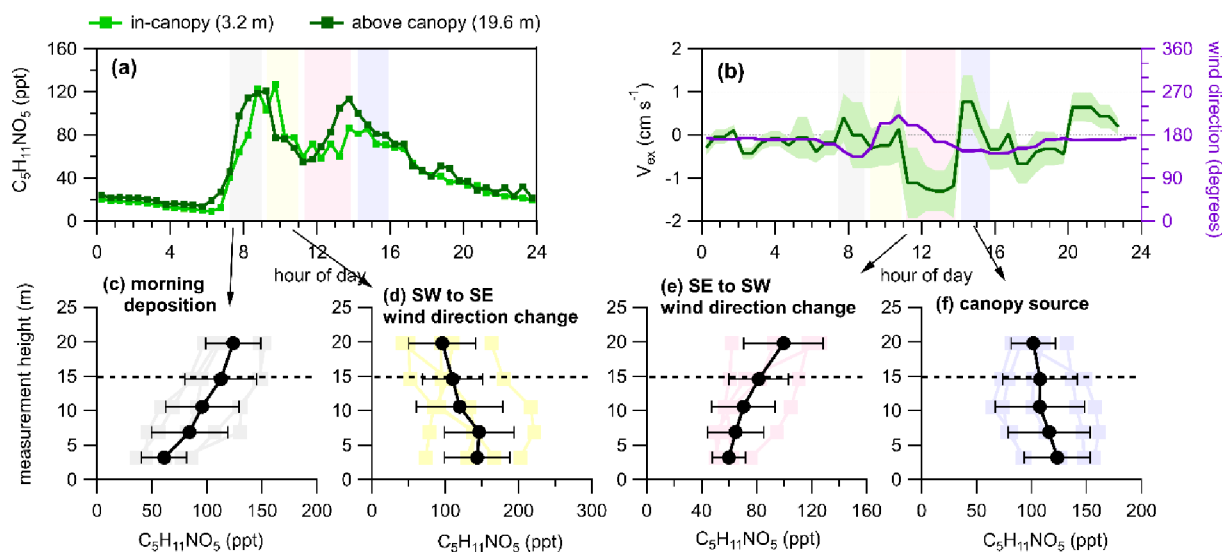


Figure 3. (a) Median $C_3H_{11}NO_5$ (MBO nitrate) concentrations at 3.2 m (in-canopy) and 19.6 m (above canopy). (b) The diel average V_{ex} values for $C_3H_{11}NO_5$ with shaded regions showing the standard deviation. The right y-axis shows the scale for wind direction (purple). The lower panels (c–f) show averages (black traces) of at least five individual representative 30 minute vertical profiles (colored traces) of $C_3H_{11}NO_5$ during the hours corresponding to the highlighted regions in panels a and b. The dotted lines in panels c–f show the approximate canopy height.

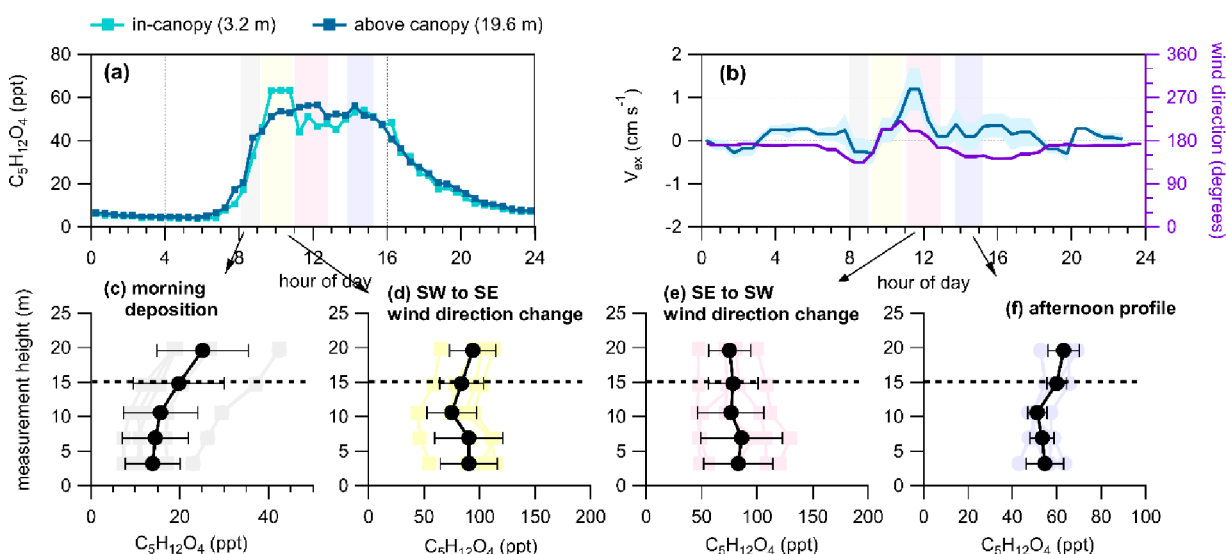


Figure 4. Diel time series of concentration (a), V_{ex} (b), and concentration vertical profiles (c–f) for $C_3H_{12}O_4$ (MBO peroxide). All the descriptions in Figure 3 apply except the lower panels correspond to gradients measured during different times than highlighted in Figure 3. The wind direction (purple) is plotted with V_{ex} .

Research and Applications version 2 (MERRA-2)⁴³ assimilated meteorology. The third simulation uses MERRA-2 meteorology for a nested simulation at $0.5^\circ \times 0.625^\circ$ from May 7th to June 10th, 2013, with a custom domain surrounding the Southern Oxidant Aerosol Study (SOAS) field study site in Talladega National Forest near Brent, AL ($\pm 4^\circ$ latitude and longitude). No changes were made to the standard model code for this run. Detailed results from the GEOS-Chem simulation can be found in Vermeuel et al. (2023).³³ Here, we only present (in Figure 5) deposition velocities (V_{dep}) from the above simulations for select OVOCs within the model grid cells containing the FluCS and SOAS field sites.

RESULTS AND DISCUSSION

Many of the OVOCs quantified in this study exhibited bidirectional vertical exchange (Figure 2). The exchange

velocity (V_{ex}) describes the rate and direction of net OVOC transfer across a plane normal to the surface at the measurement height (eq 1)

$$V_{ex} = \frac{\overline{w'x'}}{\bar{x}} \quad (1)$$

where $\overline{w'x'}$ is the covariance of vertical wind speed with the OVOC concentration, and \bar{x} is the mean OVOC concentration during the 30 min flux measurement period. Net upward exchange of OVOCs is indicated by a positive V_{ex} , while downward exchange is negative. V_{ex} values are calculated here from eddy covariance fluxes (ppt m s^{-1}) and the corresponding average concentrations (ppt) both measured above-canopy at 28 m.

We focus our analysis on data collected between 16th to 31st of August 2021 when the MEFO was not strongly impacted by

regional or transported wildfire smoke.³³ We exclude a two-day period of high cloud cover and intermittent precipitation (23rd to 25th of August). We identify two classes of compounds measured by the I⁻ CIMS that are significant for their chemical properties of reactivity and water solubility and/or potential impacts on oxidant production and budgets: peroxides/epoxides (C₅H₁₂O₄, C₅H₁₀O₃, C₂H₄O₃, and CH₄O₃) and organic nitrates (C₅H₁₁NO₅, C₅H₉NO₄, C₅H₉NO₅, and C₄H₇NO₅). These classes of OVOCs are notable as few measurements of biosphere-atmosphere exchange of them exist. Of these OVOCs, we assign C₅H₁₂O₄ and C₅H₁₁NO₅ as MBO oxidation products and the rest of the compounds as isoprene oxidation products. Above the canopy, MBO oxidation products shift between deposition and emission by time of day. Most isoprene oxidation products deposit to the forest. We hypothesize that a strong local (i.e., within the measurement footprint, see Figure S11, Vermeul et al. (2023)³³) source of MBO is responsible for some of the bidirectional exchange of MBO oxidation products because of comparable influences of chemical production and depositional loss, whereas an upwind source of isoprene produces isoprene oxidation products before they reach the footprint, where they then deposit with negligible in-canopy sources.

MBO Oxidation Products. In contrast to MBO, which showed upward flux during the day,³³ we observe bidirectional vertical exchange of MBO oxidation products throughout the day at the MEFO. The primary source of OH reactivity at the MEFO is MBO,⁴⁴ and MBO oxidation by OH should thus be an appreciable local source of OVOCs. Nearly every morning, MBO peaked at ~6 ppb between 7:00 a.m. to 10:00 a.m. (Figure S5). MBO then stabilized to ~1 ppb for the rest of the day. The I⁻ CIMS measured two analytes, observed as iodide clusters, that likely originated from MBO oxidation: C₅H₁₂O₄ (first generation MBO hydroxy hydroperoxides) and C₅H₁₁NO₅ (first generation MBO hydroxy nitrates) (Figure S6). Unlike most OVOCs observed in this study, the MBO oxidation products C₅H₁₂O₄ and C₅H₁₁NO₅ exhibited exchange velocities that changed sign (i.e., between upward/positive and downward/negative) throughout the day. Patterns in the concentration gradients of the MBO OVOCs reflect both differences in dry deposition rates and changing sources (Figures 3 and 4).

Dry deposition outcompetes production of C₅H₁₁NO₅, the MBO nitrate, for much of the day at the MEFO. The concentrations within and above the canopy (Figure 3a) are defined by an increase in the morning, followed by a decrease in the middle of the day that coincides with a pronounced decrease in the measured exchange velocities (Figure 3b). In the morning, C₅H₁₁NO₅ is likely driven by oxidation of MBO by OH and followed by reaction with NO, which is usually considerably elevated in the morning (>0.5 ppb) compared to the rest of the day (<0.1 ppb).⁴⁵ The vertical concentration profile shows considerable variability later in the morning but is consistent with chemical production competing with dry deposition (Figure 3d). In the afternoon, C₅H₁₁NO₅ is higher above the canopy than within the canopy, consistent with advection of photochemically-aged air from the upslope outflow bringing polluted air from the urban Front Range and transported C₅H₁₁NO₅. At this point, afternoon vertical concentration gradients indicate a net deposition flux.

Organic nitrates act as long-range NO_x reservoirs, and thus, biosphere-atmosphere exchange of organic nitrates can influence the regional NO_x budget.^{15,46} However, while

MBO nitrates may provide a temporary reservoir for NO_x, MBO nitrates clearly deposit to the forest, despite near-surface sources and/or in-canopy chemical production. Dry deposition of organic nitrates competes with partitioning to aerosol, where organic nitrates can undergo hydrolysis to form nitric acid, which then removes NO_x from the atmosphere.^{47,48} At the MEFO, the forest sequesters gas-phase NO_x through dry deposition of C₅H₁₁NO₅. C₅H₁₁NO₅ is relatively long-lived to OH oxidation ($\tau_{\text{OH}} \sim 6$ days; $k_{\text{OH}} = 1.75 \times 10^{-12} \text{ cm}^3 \text{ s}^{-1}$ molecules⁻¹), meaning that any molecules that are formed in the canopy and escape will likely be lost to dry deposition ($\tau_{\text{dep}} \sim 16$ h for a 1 km boundary layer height and $V_{\text{dep}} = 1.7 \text{ cm s}^{-1}$, as shown in Figure 5) downwind. Thus, MBO nitrate formation in this pine forest should be considered a permanent NO_x sink due to its fast dry deposition relative to other fates.

In contrast to C₅H₁₁NO₅, MBO peroxide (C₅H₁₂O₄) concentrations reflect local source production (Figure 4).

In the morning, a vertical gradient forms with higher C₅H₁₂O₄ concentrations above the canopy than below; V_{ex} is negative, indicating deposition and either a nonlocal source of the peroxide to the MEFO or accumulation of the peroxide in the stratified nocturnal layers above the forest overnight that then deposits in the morning. However, as a stable boundary layer forms later in the morning, increased in-canopy concentrations (Figure 4d) indicate an in-canopy source of C₅H₁₂O₄. OH oxidation of MBO forms RO₂ radicals, which then react with HO₂ to make C₅H₁₂O₄. The field measurements of DiGangi et al. (2012) from summer 2009 showed that RO₂ should dominantly react with HO₂ in the afternoon at the MEFO.⁴⁵ Our concentration gradient measurements support the hypothesis that in-canopy C₅H₁₂O₄ production outcompetes dry deposition.

Deposition to Different Forests. We calculate deposition velocities ($V_{\text{dep}} = -V_{\text{ex}}$) for select OVOC compounds measured at the MEFO, during FluCS, using the “big-leaf” resistance model of Wesely (2007) which treats the canopy as a big leaf with resistors in series. Each resistor represents a micrometeorological or biotic process that, when taken together, determine the first-order rate constant (V_{dep} , cm s⁻¹) for gaseous dry deposition:

$$V_{\text{dep}} = \frac{1}{R_a + R_b + R_c} \quad (2)$$

R_a is identical for all gases and represents the aerodynamic resistance between the surface and the measurement height; R_b is the quasilaminar sublayer resistance at the surface of a roughness element; and R_c is surface resistance modeled as a set of resistors in parallel. We calculate R_a according to the parameterization outlined in Wesely and Hicks (1977)⁴⁹ and R_b according to the parameterization of Jensen and Hummelshøj (1995).⁵⁰ Here, we focus on the treatment of the R_c term to evaluate the potential effects of solubility and reactivity on OVOC deposition. We note that our analysis does not consider contributions from soil or leaf litter. We follow the method of Nguyen et al. (2015) and assume a closed canopy. The R_c term is thus composed of stomatal (r_s), mesophilic (r_m), and cuticular (r_{cut}) resistances:

$$R_c = \frac{1}{\left(\frac{1}{r_s + r_m}\right) + \frac{1}{r_{\text{cut}}}} \quad (3)$$

The contribution of r_m to the R_c term in our study was negligible for most compounds, so we will only describe the

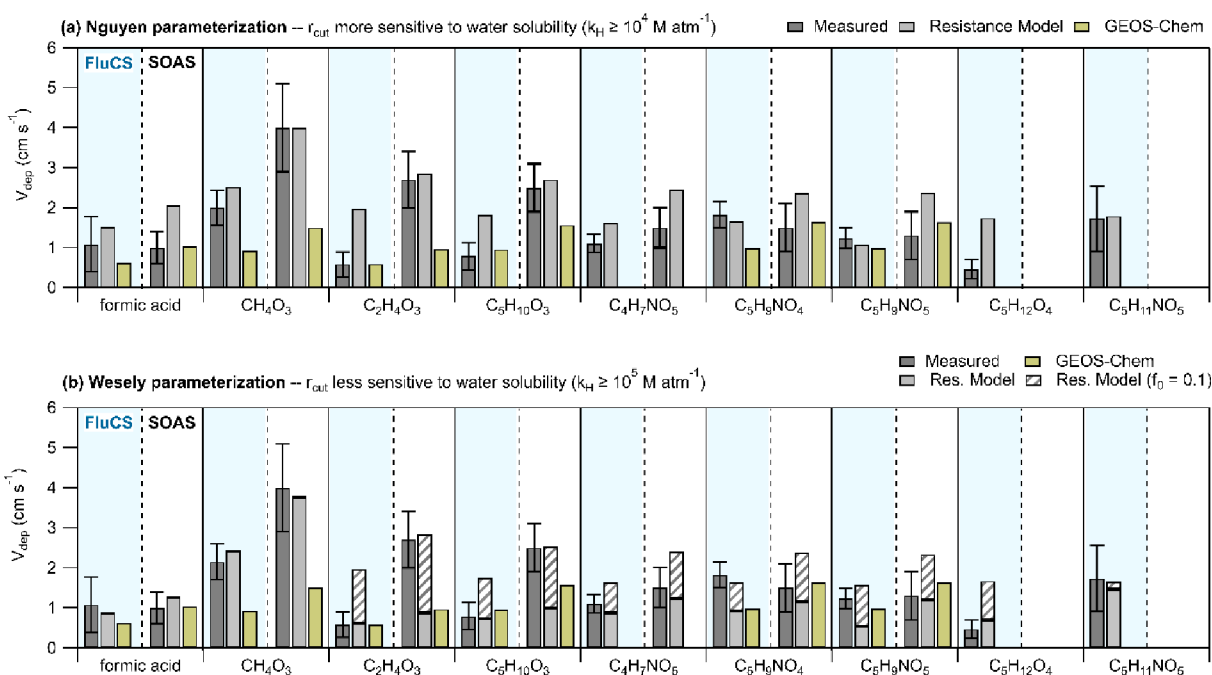


Figure 5. Mean V_{dep} values for the OVOCs measured (black) during FluCS (blue shading) and SOAS (no shading). V_{dep} values calculated from GEOS-Chem (MERRRA-2 simulations; yellow) are also shown. Error bars on the FluCS measurements are calculated similarly to Nguyen et al. (2015), representing the standard deviation of V_{dep} measured between 10:25 a.m. and 4:45 p.m. (a) The resistance model values using the Wesely parameterization modified for increased water solubility sensitivity to the cuticular resistance (r_{cut}), as presented by Nguyen et al. (2015). (b) The resistance model values were calculated using the original Wesely parameterization (Wesely, 2007). The striped bar sections show how V_{dep} is increased when the reactivity factor (f_0) is equal to 0.1.

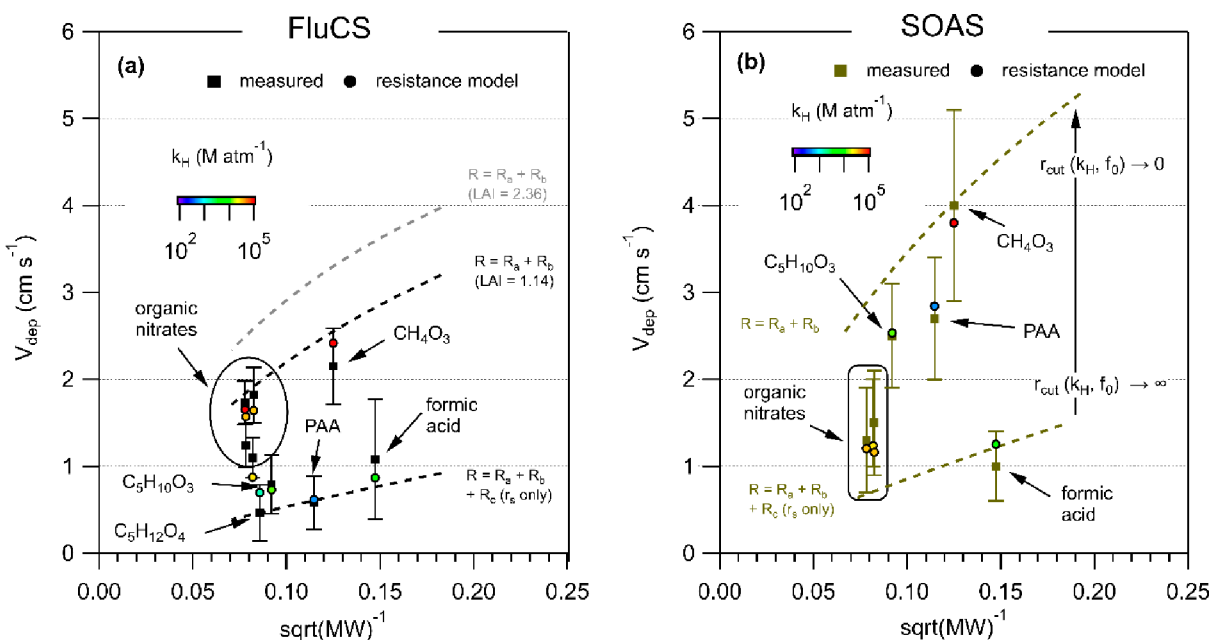


Figure 6. V_{dep} as a function of the inverse square root of the molecular weight (MW) is shown for HCOOH , CH_4O_3 , $\text{C}_2\text{H}_4\text{O}_3$, $\text{C}_3\text{H}_{10}\text{O}_3$, $\text{C}_4\text{H}_7\text{NO}_5$, $\text{C}_5\text{H}_9\text{NO}_4$, $\text{C}_5\text{H}_9\text{NO}_5$, $\text{C}_5\text{H}_{12}\text{O}_4$, and $\text{C}_5\text{H}_{11}\text{NO}_5$ for measured (solid squares) and resistance model (solid circles) values from FluCS (a) and SOAS (b). The representation of V_{dep} as a function of MW was originally presented by Nguyen et al. (2015). $\text{C}_5\text{H}_{12}\text{O}_5$ and $\text{C}_5\text{H}_{11}\text{NO}_5$ were not measured during SOAS. The color of the resistance model values shows Henry's Law constant (10^2 M atm^{-1} is the lower limit, blue; 10^5 M atm^{-1} is the upper limit, red) used herein. The dashed lines with higher V_{dep} show the upper limit for deposition without surface resistance ($R_a + R_b$). We show an additional calculation of the upper V_{dep} limit for FluCS to demonstrate the uncertainty associated with LAI. The dashed lines with lower V_{dep} show the lower limit for deposition when V_{dep} is controlled by high cuticular resistance ($R_a + R_b + R_c$ (i.e., r_s only case)). The direction of the arrow shows that when cuticular resistance (r_{cut}) decreases, the V_{dep} increases beyond the lower limit controlled by stomatal uptake. A value of $f_0 = 0.1$ is applied to organic nitrates for FluCS and to peroxide/epoxides for SOAS.

effects of stomatal and cuticular resistance contributions to the surface resistance. Both the R_b and r_s terms depend on the gaseous diffusivity of an OVOC, and thus, through Graham's Law (i.e., $D_x = D_{\text{H}_2\text{O}} \sqrt{\frac{MW_{\text{H}_2\text{O}}}{MW_{\text{OVOC}}}}$; where D is the gaseous diffusivity and MW is the molecular weight of an OVOC or water), both terms are directly proportional to the MW of an OVOC. The stomatal resistance models how efficiently an OVOC can diffuse into leaf stomata relative to water vapor.

We expect OVOC deposition to vary with forest types. To investigate the role of forest type in controlling OVOC deposition, we compare V_{dep} for select OVOC compounds measured at the MEFO, during FluCS, to the same compounds measured by Nguyen et al. (2015) over the Talladega National Forest (TNF) during the Southeastern Oxidant and Aerosol Study (SOAS; summer 2013) and to resistance-model calculated V_{dep} from GEOS-Chem (Figure 5).

These forests differ by composition (The MEFO is a pine forest; the TNF is a mixed broadleaf and coniferous forest.), canopy denseness (The MEFO is a sparse canopy; the TNF is dense.), and climate (The MEFO is arid; the TNF is humid and subtropical). V_{dep} values measured from the MEFO (Table S3) are generally consistent within a given class of molecules with values falling within 25% for peroxides/epoxides (except for hydroxy methyl hydroperoxide, HMHP, CH_4O_3) and within 30% for organic nitrates. The measured V_{dep} values for organic nitrates fall within the range of literature values for organic nitrate fluxes.^{9,26} Our MEFO V_{dep} values for peroxides/epoxides generally fall on the lower end of previous reported ranges.^{26,51} Overall, despite the different compositions and climates of these two forests, most OVOC V_{dep} values measured during FluCS and SOAS agree within the range of reported error. Notable exceptions include CH_4O_3 , $\text{C}_2\text{H}_4\text{O}_3$, and $\text{C}_5\text{H}_{10}\text{O}_3$, all of which have higher deposition velocities at SOAS compared to FluCS.

To investigate why some OVOC V_{dep} agreed well between the two sites and others did not, we compared resistance model V_{dep} for FluCS versus SOAS (Figure 5, black bars). We also compared these V_{dep} values to those used by GEOS-Chem in model simulations (Figure 5, gold bars). For FluCS, GEOS-Chem either underpredicts or overpredicts by more than 20% with the Wesely resistance model V_{dep} (with $f_0 = 0.1$ for organic nitrates) for all compounds except $\text{C}_2\text{H}_4\text{O}_3$. GEOS-Chem calculates V_{dep} from a "big leaf" resistance model that determines the surface resistance (R_c) as a function of LAI and photosynthetically active radiation. Nguyen et al. (2015) modified cuticular and mesophilic resistance elements, increasing sensitivity to water solubility and bringing model V_{dep} values into agreement with measurements. The V_{dep} predicted from the Nguyen resistance model agrees with SOAS measurements but not with the GEOS-Chem predictions for the peroxides/epoxides (CH_4O_3 , $\text{C}_2\text{H}_4\text{O}_3$, and $\text{C}_3\text{H}_{10}\text{O}_3$). This discrepancy suggests that the Nguyen et al. (2015) optimization of the Wesely "big-leaf" resistance model for gaseous dry deposition may have been appropriate for the SOAS ecosystem but not for other sites. Taken another way, our FluCS data is not consistent with the strong role of solubility in determining V_{dep} suggested by Nguyen et al. (2015).

Previous studies have proposed that OVOC V_{dep} can be parameterized simply as a function of MW.^{37,26} Thus, we use our resistance model for three cases to describe a range of

useful upper and lower limits for OVOC V_{dep} as a function of MW (Figure 6).

The first case describes the upper limit of gaseous V_{dep} , in which deposition occurs with negligible surface resistance (i.e., $R_c \rightarrow 0 \text{ s cm}^{-1}$) and is determined by the R_a and R_b terms. Nguyen et al. (2015) showed that prototypical molecules for deposition with no surface resistance (e.g., the aerodynamic limit) included nitric acid, hydrogen peroxide, and HMHP. Compared to this V_{dep} upper limit for FluCS and SOAS, the maximum rate at which OVOCs can deposit is highly dependent on LAI, and thus, the upper limit for SOAS is higher than the MEFO. The TNF is dense with an LAI of $4.7 \text{ m}^2 \text{ m}^{-2}$, whereas the MEFO pine forest is sparse and has a previously reported³¹ LAI of $1.14 \text{ m}^2 \text{ m}^{-2}$ and a recently determined value³³ of $2.36 \text{ m}^2 \text{ m}^{-2}$. We show how these two LAI values for FluCS shift the V_{dep} upper limit calculated for FluCS (Figure 6a, gray dashed line). Differences in LAI have a large effect on predicted V_{dep} and represent a substantial uncertainty in our analysis. However, it is clear that sticky OVOCs that are not subject to surface resistance will deposit more quickly at SOAS than at the MEFO. For example, $\text{C}_5\text{H}_{11}\text{NO}_5$ deposited at the aerodynamic limit during FluCS, whereas HMHP deposited at aerodynamic limit for SOAS.

The second case describes the lower limit for OVOC V_{dep} , in which molecules experience high cuticular resistance (i.e., $r_{\text{cut}} \rightarrow \infty$) and will only deposit at a rate that is limited by diffusion into stomata (r_s). r_s is dependent on water vapor concentrations ($[\text{H}_2\text{O}]_g$, mmol m^{-3}) and the stomatal conductance to water (g_s)

$$r_s = \left(\frac{D_{\text{H}_2\text{O}}}{D_x} \right) \frac{[\text{H}_2\text{O}]_g}{g_s} \quad (4)$$

where g_s is a measure of how open the stomata of the leaves are. For this case, if molecules experience high cuticular resistance, they will deposit faster at the TNF compared to the MEFO. This trend is explained by a higher stomatal resistance to water vapor at the MEFO compared to the TNF (i.e., $\frac{[\text{H}_2\text{O}]_g}{g_s}$

for MEFO > TNF). Our value for g_s , $5 \text{ mmol m}^{-2} \text{ s}^{-1}$, is the campaign average from needle-level measurements. If the g_s value was similar to previous reports (e.g., $30 \text{ mmol m}^{-2} \text{ s}^{-1}$),³¹ we would expect molecules at the high cuticular resistance limit to deposit faster. At FluCS, $\text{C}_2\text{H}_4\text{O}_3$, $\text{C}_5\text{H}_{10}\text{O}_3$, $\text{C}_5\text{H}_{12}\text{O}_4$, and formic acid, all have measured V_{dep} close to the lower V_{dep} "high cuticular resistance" limit. In contrast, at SOAS, formic acid was the only molecule that deposited near the "high cuticular resistance" limit; however, the strong upward flux of formic acid measured during both SOAS and FluCS acts as a systematic offset in the determination of V_{dep} .

The third case varies the reactivity factor (f_0 ; a number between 0 and 1 describing how reactive an OVOC is within the cuticle compared to ozone) to be non-zero and/or the Henry's Law constant (k_H) to be between 10^2 and 10^5 M atm^{-1} (Figure 6, coloring on resistance model markers). In this case, the lower limit to V_{dep} that is created by stomatal resistance is now increased due to reactions or aqueous uptake into leaf cuticles. In other words, R_c is decreased as r_{cut} decreases (Figure 6) and depends on OVOC reactivity and solubility as described from the original Wesely parameterization:

$$r_{\text{cut}} = \frac{1}{10^{-5}k_{\text{H}} + f_0} \quad (5)$$

Nguyen et al. (2015) updated the treatment of r_{cut} to decrease the threshold for which solubility begins to be important in affecting r_{cut} (eq 6).

$$r_{\text{cut}} = \frac{1}{\left(\frac{10^{-4}k_{\text{H}}}{RT}\right) + f_0} \quad (6)$$

From eq 6, R is the ideal gas constant, and T is temperature. Within the Nguyen et al. (2015) updated framework, molecules with a $k_{\text{H}} < 10^2 \text{ M atm}^{-1}$ will deposit at the “high cuticular resistance” V_{dep} lower limit, while molecules with a $k_{\text{H}} > 10^4 \text{ M atm}^{-1}$ will deposit at the aerodynamic limit.

For many of the molecules under consideration here, k_{H} has not been directly measured. Recent measurements for 1,2-ISOPOOH⁵² and 1,4-isoprene hydroxynitrate (an isomer of $\text{C}_5\text{H}_9\text{NO}_4$)¹⁵ show that the ISOPOOH isomer is less soluble than previously assumed by Nguyen et al. (2015), while the measured $\text{C}_5\text{H}_9\text{NO}_4$ isomer is more soluble (Table S2). Figures 5 and 6 show V_{dep} predictions from our resistance model for FluCS and SOAS using updated k_{H} values (Table S2 for details). Our analysis ignores the isomeric composition of the OVOC population, causing substantial uncertainty in our assumed k_{H} values. However, we see that the increased sensitivity to solubility proposed by Nguyen et al. (2015) overpredicts V_{dep} for the organic nitrates at SOAS (Figure 5a) and three peroxide/epoxide species at FluCS ($\text{C}_5\text{H}_{10}\text{O}_3$, $\text{C}_5\text{H}_{12}\text{O}_4$, and $\text{C}_2\text{H}_4\text{O}_3$).

The original Wesely solubility threshold (10^5 M atm^{-1}) gives better model-measurement agreement (Figure 5b) than the updated solubility threshold (10^4 M atm^{-1}) proposed by Nguyen et al. (2015) for almost all OVOCs at both campaigns. The notable exceptions are the two peroxides/epoxides at SOAS ($\text{C}_5\text{H}_{10}\text{O}_3$ and $\text{C}_2\text{H}_4\text{O}_3$) and two organic nitrates at FluCS ($\text{C}_5\text{H}_9\text{NO}_4$ and $\text{C}_5\text{H}_9\text{NO}_5$). In both cases, V_{dep} is underpredicted. We propose that this underprediction is due to surface reactivity, as described by the reactivity factor (f_0). The patterned portions of the bars in Figure 5b show how V_{dep} increases for $f_0 = 0.1$ (10% as a reactive as ozone in the cuticle) versus $f_0 = 0$. Using a $f_0 = 0.1$ brings V_{dep} for $\text{C}_5\text{H}_{10}\text{O}_3$ and $\text{C}_2\text{H}_4\text{O}_3$ (SOAS) and $\text{C}_5\text{H}_9\text{NO}_4$ and $\text{C}_5\text{H}_9\text{NO}_5$ (FluCS) into better agreement with measurements. We thus assign an $f_0 = 0.1$ in the original Wesely derivation of the resistance model for these compounds (Figure 6). Applying a reactivity factor to $\text{C}_4\text{H}_7\text{NO}_5$ (likely a ketone or aldehyde hydroxy nitrate)⁵³ does not improve model/measurement agreement, suggesting that reactive uptake of organic nitrates is limited to compounds without additional ketone or aldehyde functionalities.

The reactivity factor reconciles our resistance model with deposition measurements and points to a reactive uptake mechanism in broadleaf vegetation for peroxides/epoxides²² and pine needles for alkyl nitrates.⁵⁴ Canaval et al. (2020) reported reduction of ISOPOOH to methyl ethyl ketone (MEK) in broadleaf poplar leaves. Place et al. (2022) reported stomatal uptake and subsequent mesophilic processing of alkyl nitrates to pine needles, which could explain the need for a reactivity term for organic nitrates at FluCS. The Wesely resistance model is typically insensitive to mesophilic resistance, so we assign the reactivity for organic nitrates as a cuticular process. More fumigation studies of plants could

provide insight into mechanisms of OVOC uptake to (and emission from) plants.

The MBO oxidation products showed evidence of in-canopy chemistry in the gradient measurements that resulted in an upward flux contribution to the exchange velocity. This chemistry-induced upward flux may have occurred persistently and thus cannot be decoupled from our estimates of deposition velocity. Like the MBO oxidation products, the other OVOCs could have a chemistry-driven emission source that would systematically bias our deposition velocity estimates low. In other words, the MBO OVOC in-canopy source would need to be completely inactive to get a true measure of V_{dep} . To consider the effect of this bias on the interpretation of our results, we can consider an extreme example. If we increase V_{dep} measured from FluCS for $\text{C}_2\text{H}_4\text{O}_3$, $\text{C}_5\text{H}_{10}\text{O}_3$, and $\text{C}_5\text{H}_{12}\text{O}_4$ by 50% (the approximate relative uncertainty on measured V_{dep} for the peroxides/epoxides), then it is possible the increased sensitivity of r_{cut} to water solubility proposed by Nguyen et al. (2015) could explain deposition for $\text{C}_5\text{H}_{10}\text{O}_3$ but not for $\text{C}_2\text{H}_4\text{O}_3$ or $\text{C}_5\text{H}_{12}\text{O}_4$. On the other hand, if we increase the measured V_{dep} for organic nitrates ($\text{C}_5\text{H}_9\text{NO}_4$ and $\text{C}_5\text{H}_9\text{NO}_5$) by 20% (the approximate relative V_{dep} uncertainty for $\text{C}_5\text{H}_9\text{NO}_4$ and $\text{C}_5\text{H}_9\text{NO}_5$), increased sensitivity of r_{cut} to water solubility alone slightly underpredicts (29% for $\text{C}_5\text{H}_9\text{NO}_4$ and 39% for $\text{C}_5\text{H}_9\text{NO}_5$) deposition of the organic nitrates at FluCS. Here, we have identified the potential importance of reactive uptake for organic nitrates at the MEFO and peroxides/epoxides at SOAS, but the combined uncertainties of our measurement and resistance model still allow for the possibility that solubility could play a more important role in regulating OVOC deposition than assumed in the original Wesely r_{cut} parameterization.

CONCLUSIONS

Vertical gradients and fluxes of MBO and isoprene oxidation products over a pine forest highlight features of bidirectional OVOC exchange driven by deposition, reactive uptake on leaf surfaces, and in-canopy chemistry. Plant composition and climate differences regulate OVOC deposition, with the pine forests taking up several organic nitrates, and surface moisture at the more humid mixed forest site enhanced peroxide deposition. Larger LAI at the mixed broadleaf forest increased the upper limit of V_{dep} , highlighting the importance of accurate measurements (and models) of LAI across land use types. For OVOCs that experience either no surface resistance (upper V_{dep} limit), or high cuticular resistance (lower V_{dep} limit), V_{dep} can be approximated as a function of $\text{sqrt}(\text{MW})^{-1}$. We propose that there is a reactive uptake mechanism for hydroxy nitrates to pine needles—and that vegetation-dependent reactivity explains the rapid OVOC dry deposition observed both at FluCS and previously at SOAS, rather than the previously-proposed solubility mechanism. Future measurements of canopy-scale OVOC concentration gradients in ecosystems with vegetation types and climates that add to the types of ecosystems highlighted in our work, and the work of Nguyen et al. (2015), could be used to further constrain the role of solubility and surface reactivity in regulating their deposition flux.

GEOS-Chem predicted V_{dep} well (within 25% of measured values) for most compounds at FluCS. We see a clear need to understand the mechanisms of OVOC deposition across different climate and forest types, as it determines the lifetime of OVOCs in the atmosphere.

For example, Singh et al. (2004) originally proposed an unexplained global biogenic source of methyl ethyl ketone⁵⁵ that was recently nearly reconciled as ISOPOOH deposition and subsequent methyl ethyl ketone production and emission over broadleaf vegetation.²² Such processes may be at play with other OVOCs, such as the peroxide/epoxide and organic nitrate cases described here.

■ ASSOCIATED CONTENT

SI Supporting Information

The Supporting Information is available free of charge at <https://pubs.acs.org/doi/10.1021/acsestair.3c00074>.

Additional experimental details, materials, and methods, including supplementary analyses and calibration procedures (PDF)

■ AUTHOR INFORMATION

Corresponding Author

Delphine K. Farmer – Department of Chemistry, Colorado State University, Fort Collins, Colorado 80523, United States; orcid.org/0000-0002-6470-9970;
Email: delphine.farmer@colostate.edu

Authors

Michael F. Link – Department of Chemistry, Colorado State University, Fort Collins, Colorado 80523, United States; Present Address: Engineering Laboratory, National Institute of Standards and Technology, Gaithersburg, MD 20899, USA; orcid.org/0000-0002-1841-2455
Matson A. Pothier – Department of Chemistry, Colorado State University, Fort Collins, Colorado 80523, United States
Michael P. Vermeuel – Department of Soil, Water, and Climate, University of Minnesota, St. Paul, Minnesota 55455, United States; orcid.org/0000-0001-8751-0027
Mj Riches – Department of Chemistry, Colorado State University, Fort Collins, Colorado 80523, United States
Dylan B. Millet – Department of Soil, Water, and Climate, University of Minnesota, St. Paul, Minnesota 55455, United States; orcid.org/0000-0003-3076-125X

Complete contact information is available at: <https://pubs.acs.org/doi/10.1021/acsestair.3c00074>

Notes

The authors declare no competing financial interest.

■ ACKNOWLEDGMENTS

We thank the Flux Closure Study (FluCS) team, including Sara Williams, Emily Reidy, Paige Price, Brandon Bottorff, Lindsay Halleckson, and Phillip Stevens, for their constructive input and collaboration. We acknowledge the National Science Foundation (AGS-1932849) and the Alfred P. Sloan Foundation (G-2018-11130) for funding. We thank NCAR for tower maintenance and Paula Fornwalt and Steve Alton from USFS for support during the campaign. We thank Tran Nguyen for providing SOAS data and for a helpful discussion.

■ REFERENCES

(1) Heald, C. L.; Gouw, J. d.; Goldstein, A. H.; Guenther, A. B.; Hayes, P. L.; Hu, W.; Isaacman-VanWertz, G.; Jimenez, J. L.; Keutsch, F. N.; Koss, A. R.; et al. Contrasting Reactive Organic Carbon Observations in the Southeast United States (SOAS) and Southern

California (CalNex). *Environ. Sci. Technol.* **2020**, *54* (23), 14923–14935.

(2) Millet, D. B.; Alwe, H. D.; Chen, X.; Deventer, M. J.; Griffis, T. J.; Holzinger, R.; Bertman, S. B.; Rickly, P. S.; Stevens, P. S.; Léonardis, T.; et al. Bidirectional ecosystem-atmosphere fluxes of volatile organic compounds across the mass spectrum: How many matter? *ACS Earth and Space Chemistry* **2018**, *2* (8), 764–777.

(3) Farmer, D. K.; Riches, M. Measuring biosphere-atmosphere exchange of short-lived climate forcers and their precursors. *Acc. Chem. Res.* **2020**, *53* (8), 1427–1435.

(4) Knote, C.; Hodzic, A.; Jimenez, J. The effect of dry and wet deposition of condensable vapors on secondary organic aerosols concentrations over the continental US. *Atmospheric Chemistry and Physics* **2015**, *15* (1), 1–18.

(5) Kaser, L.; Karl, T.; Guenther, A.; Graus, M.; Schnitzhofer, R.; Turnipseed, A.; Fischer, L.; Harley, P.; Madronich, M.; Gochis, D.; et al. Undisturbed and disturbed above canopy ponderosa pine emissions: PTR-TOF-MS measurements and MEGAN 2.1 model results. *Atmospheric Chemistry and Physics* **2013**, *13* (23), 11935–11947.

(6) Schallhart, S.; Rantala, P.; Kajos, M. K.; Aalto, J.; Mammarella, I.; Ruuskanen, T. M.; Kulmala, M. Temporal variation of VOC fluxes measured with PTR-TOF above a boreal forest. *Atmospheric Chemistry and Physics* **2018**, *18* (2), 815–832.

(7) Park, J.-H.; Fares, S.; Weber, R.; Goldstein, A. Biogenic volatile organic compound emissions during BEARPEX 2009 measured by eddy covariance and flux-gradient similarity methods. *Atmospheric Chemistry and Physics* **2014**, *14* (1), 231–244.

(8) Farmer, D.; Wooldridge, P.; Cohen, R. Application of thermal-dissociation laser induced fluorescence (TD-LIF) to measurement of HNO₃, alkyl nitrates, peroxy nitrates, and NO₂ fluxes using eddy covariance. *Atmospheric Chemistry and Physics* **2006**, *6* (11), 3471–3486.

(9) Farmer, D.; Cohen, R. Observations of HNO₃, ΣAN, ΣPN and NO₂ fluxes: evidence for rapid HO_x chemistry within a pine forest canopy. *Atmospheric Chemistry and Physics* **2008**, *8* (14), 3899–3917.

(10) Schobesberger, S.; Lopez-Hilfiker, F. D.; Taipale, D.; Millet, D. B.; D'Ambro, E. L.; Rantala, P.; Mammarella, I.; Zhou, P.; Wolfe, G. M.; Lee, B. H.; et al. High upward fluxes of formic acid from a boreal forest canopy. *Geophysical Research Letters* **2016**, *43* (17), 9342–9351.

(11) Fulgham, S. R.; Brophy, P.; Link, M.; Ortega, J.; Pollack, I.; Farmer, D. K. Seasonal flux measurements over a Colorado pine forest demonstrate a persistent source of organic acids. *ACS Earth and Space Chemistry* **2019**, *3* (9), 2017–2032.

(12) Vermeuel, M. P.; Cleary, P. A.; Desai, A. R.; Bertram, T. H. Simultaneous Measurements of O₃ and HCOOH Vertical Fluxes Indicate Rapid In-Canopy Terpene Chemistry Enhances O₃ Removal Over Mixed Temperate Forests. *Geophysical Research Letters* **2021**, *48* (3), No. e2020GL090996.

(13) Alwe, H. D.; Millet, D. B.; Chen, X.; Raff, J. D.; Payne, Z. C.; Fledderman, K. Oxidation of volatile organic compounds as the major source of formic acid in a mixed forest canopy. *Geophysical research letters* **2019**, *46* (5), 2940–2948.

(14) Wei, D.; Alwe, H. D.; Millet, D. B.; Bottorff, B.; Lew, M.; Stevens, P. S.; Shutter, J. D.; Cox, J. L.; Keutsch, F. N.; Shi, Q.; et al. FORest Canopy Atmosphere Transfer (FORCAST) 2.0: model updates and evaluation with observations at a mixed forest site. *Geoscientific Model Development* **2021**, *14* (10), 6309–6329.

(15) Vasquez, K. T.; Crounse, J. D.; Schulze, B. C.; Bates, K. H.; Teng, A. P.; Xu, L.; Allen, H. M.; Wennberg, P. O. Rapid hydrolysis of tertiary isoprene nitrate efficiently removes NO_x from the atmosphere. *Proc. Natl. Acad. Sci. U. S. A.* **2020**, *117* (52), 33011–33016.

(16) Bates, K. H.; Jacob, D. J. A new model mechanism for atmospheric oxidation of isoprene: global effects on oxidants, nitrogen oxides, organic products, and secondary organic aerosol. *Atmospheric Chemistry and Physics* **2019**, *19* (14), 9613–9640.

(17) Link, M. F.; Brophy, P.; Fulgham, S. R.; Murschell, T.; Farmer, D. K. Isoprene versus Monoterpenes as Gas-Phase Organic Acid

Precursors in the Atmosphere. *ACS Earth and Space Chemistry* **2021**, *5* (6), 1600–1612.

(18) Hicks, B. B.; Saylor, R. D.; Baker, B. D. Dry deposition of particles to canopies—A look back and the road forward. *Journal of Geophysical Research: Atmospheres* **2016**, *121* (24), 14691–14707.

(19) Wennberg, P. O.; Bates, K. H.; Crouse, J. D.; Dodson, L. G.; McVay, R. C.; Mertens, L. A.; Nguyen, T. B.; Praske, E.; Schwantes, R. H.; Smarte, M. D.; et al. Gas-phase reactions of isoprene and its major oxidation products. *Chem. Rev.* **2018**, *118* (7), 3337–3390.

(20) Wu, Z.; Zhang, L.; Walker, J. T.; Makar, P. A.; Perlinger, J. A.; Wang, X. Extension of a gaseous dry deposition algorithm to oxidized volatile organic compounds and hydrogen cyanide for application in chemistry transport models. *Geoscientific Model Development* **2021**, *14* (8), 5093–5105.

(21) Clifton, O. E.; Patton, E. G.; Barth, M.; Orlando, J.; Wang, S.; Baublitz, C. Influence of organized turbulence on OH reactivity at a deciduous forest. *Geophysical Research Letters* **2023**, *50* (7), No. e2022GL102548.

(22) Canaval, E.; Millet, D. B.; Zimmer, I.; Nosenko, T.; Georgii, E.; Partoll, E. M.; Fischer, L.; Alwe, H. D.; Kulmala, M.; Karl, T.; et al. Rapid conversion of isoprene photooxidation products in terrestrial plants. *Communications earth & environment* **2020**, *1* (1), 1–9.

(23) Dibley, M.; Jaffe, A.; O'Brien, R. E. Molecular Insights into Dissolved Organic Matter in Natural Dew Water: Biogrimme Films on Leaf Surfaces. *ACS Earth and Space Chemistry* **2022**, *6* (3), 775–787.

(24) Fulgham, S.; Millet, D.; Alwe, H.; Goldstein, A.; Schobesberger, S.; Farmer, D. Surface wetness as an unexpected control on forest exchange of volatile organic acids. *Geophysical Research Letters* **2020**, *47* (15), No. e2020GL088745.

(25) Forkel, R.; Guenther, A.; Ashworth, K.; Bedos, C.; Delon, C.; Lathiere, J.; Noe, S.; Potier, E.; Rinne, J.; Tchepel, O.; et al. Bidirectional exchange of volatile organic compounds. *Review and integration of biosphere-atmosphere modelling of reactive trace gases and volatile aerosols* **2015**, 169–179.

(26) Nguyen, T. B.; Crouse, J. D.; Teng, A. P.; St. Clair, J. M.; Paulot, F.; Wolfe, G. M.; Wennberg, P. O. Rapid deposition of oxidized biogenic compounds to a temperate forest. *Proc. Natl. Acad. Sci. U. S. A.* **2015**, *112* (5), E392–E401.

(27) Wolfe, G.; Thornton, J.; McKay, M.; Goldstein, A. Forest-atmosphere exchange of ozone: sensitivity to very reactive biogenic VOC emissions and implications for in-canopy photochemistry. *Atmospheric Chemistry and Physics* **2011**, *11* (15), 7875–7891.

(28) Guenther, A.; Karl, T.; Harley, P.; Wiedinmyer, C.; Palmer, P. I.; Geron, C. Estimates of global terrestrial isoprene emissions using MEGAN (Model of Emissions of Gases and Aerosols from Nature). *Atmospheric Chemistry and Physics* **2006**, *6* (11), 3181–3210.

(29) Harley, P.; Fridd-Stroud, V.; Greenberg, J.; Guenther, A.; Vasconcellos, P. Emission of 2-methyl-3-buten-2-ol by pines: A potentially large natural source of reactive carbon to the atmosphere. *Journal of Geophysical Research: Atmospheres* **1998**, *103* (D19), 25479–25486.

(30) Wolfe, G.; Hanisco, T.; Arkinson, H.; Bui, T.; Crouse, J.; Dean-Day, J.; Goldstein, A.; Guenther, A.; Hall, S.; Huey, G.; et al. Quantifying sources and sinks of reactive gases in the lower atmosphere using airborne flux observations. *Geophysical Research Letters* **2015**, *42* (19), 8231–8240.

(31) Ortega, J.; Turnipseed, A.; Guenther, A. B.; Karl, T. G.; Day, D.; Gochis, D.; Huffman, J.; Prenni, A. J.; Levin, E.; Kreidenweis, S. M.; et al. Overview of the Manitou Experimental Forest Observatory: site description and selected science results from 2008 to 2013. *Atmospheric Chemistry and Physics* **2014**, *14* (12), 6345–6367.

(32) Kim, S.; Karl, T.; Guenther, A.; Tyndall, G.; Orlando, J.; Harley, P.; Rasmussen, R.; Apel, E. Emissions and ambient distributions of Biogenic Volatile Organic Compounds (BVOC) in a ponderosa pine ecosystem: interpretation of PTR-MS mass spectra. *Atmospheric Chemistry and Physics* **2010**, *10* (4), 1759–1771.

(33) Vermeuel, M. P.; Millet, D. B.; Farmer, D. K.; Pothier, M. A.; Link, M. F.; Riches, M.; Williams, S.; Garofalo, L. A. Closing the reactive carbon flux budget: Observations from dual mass

spectrometers over a coniferous forest. *Journal of Geophysical Research: Atmospheres* **2023**, *128*, e2023JD038753.

(34) Bi, C.; Krechmer, J. E.; Frazier, G. O.; Xu, W.; Lambe, A. T.; Clafin, M. S.; Lerner, B. M.; Jayne, J. T.; Worsnop, D. R.; Canagaratna, M. R.; et al. Quantification of isomer-resolved iodide chemical ionization mass spectrometry sensitivity and uncertainty using a voltage-scanning approach. *Atmospheric Measurement Techniques* **2021**, *14* (10), 6835–6850.

(35) Horst, T. A simple formula for attenuation of eddy fluxes measured with first-order-response scalar sensors. *Boundary-Layer Meteorology* **1997**, *82*, 219–233.

(36) Bariteau, L.; Helmig, D.; Fairall, C.; Hare, J.; Hueber, J.; Lang, E. Determination of oceanic ozone deposition by ship-borne eddy covariance flux measurements. *Atmospheric Measurement Techniques* **2010**, *3* (2), 441–455.

(37) Wesely, M. Parameterization of surface resistances to gaseous dry deposition in regional-scale numerical models. *Atmospheric Environment* **2007**, *41*, 52–63.

(38) Bey, I.; Jacob, D. J.; Yantosca, R. M.; Logan, J. A.; Field, B. D.; Fiore, A. M.; Li, Q.; Liu, H. Y.; Mickley, L. J.; Schultz, M. G. Global modeling of tropospheric chemistry with assimilated meteorology: Model description and evaluation. *Journal of Geophysical Research: Atmospheres* **2001**, *106* (D19), 23073–23095.

(39) Wang, Y.; Jacob, D. J.; Logan, J. A. Global simulation of tropospheric O₃-NO_x-hydrocarbon chemistry: 1. Model formulation. *Journal of Geophysical Research: Atmospheres* **1998**, *103* (D9), 10713–10725.

(40) Karl, T.; Harley, P.; Emmons, L.; Thornton, B.; Guenther, A.; Basu, C.; Turnipseed, A.; Jardine, K. Efficient atmospheric cleansing of oxidized organic trace gases by vegetation. *Science* **2010**, *330* (6005), 816–819.

(41) Myneni, R. B.; Hoffman, S.; Knyazikhin, Y.; Privette, J.; Glassy, J.; Tian, Y.; Wang, Y.; Song, X.; Zhang, Y.; Smith, G.; et al. Global products of vegetation leaf area and fraction absorbed PAR from year one of MODIS data. *Remote sensing of environment* **2002**, *83* (1-2), 214–231.

(42) Olson, D. M.; Dinerstein, E.; Wikramanayake, E. D.; Burgess, N. D.; Powell, G. V.; Underwood, E. C.; D'Amico, J. A.; Itoua, I.; Strand, H. E.; Morrison, J. C.; et al. Terrestrial Ecoregions of the World: A New Map of Life on Earth: A new global map of terrestrial ecoregions provides an innovative tool for conserving biodiversity. *BioScience* **2001**, *51* (11), 933–938.

(43) Gelaro, R.; McCarty, W.; Suárez, M. J.; Todling, R.; Molod, A.; Takacs, L.; Randles, C. A.; Darmenov, A.; Bosilovich, M. G.; Reichle, R.; et al. The modern-era retrospective analysis for research and applications, version 2 (MERRA-2). *Journal of climate* **2017**, *30* (14), 5419–5454.

(44) Hunter, J. F.; Day, D. A.; Palm, B. B.; Yatavelli, R. L.; Chan, A. W.; Kaser, L.; Cappellin, L.; Hayes, P. L.; Cross, E. S.; Carrasquillo, A. J.; et al. Comprehensive characterization of atmospheric organic carbon at a forested site. *Nature Geoscience* **2017**, *10* (10), 748–753.

(45) DiGangi, J.; Henry, S.; Kamrath, A.; Boyle, E.; Kaser, L.; Schnitzhofer, R.; Graus, M.; Turnipseed, A.; Park, J.; Weber, R.; et al. Observations of glyoxal and formaldehyde as metrics for the anthropogenic impact on rural photochemistry. *Atmospheric Chemistry and Physics* **2012**, *12* (20), 9529–9543.

(46) Perring, A.; Pusede, S.; Cohen, R. An observational perspective on the atmospheric impacts of alkyl and multifunctional nitrates on ozone and secondary organic aerosol. *Chem. Rev.* **2013**, *113* (8), 5848–5870.

(47) Zare, A.; Fahey, K. M.; Sarwar, G.; Cohen, R. C.; Pye, H. O. Vapor-pressure pathways initiate but hydrolysis products dominate the aerosol estimated from organic nitrates. *ACS Earth and Space Chemistry* **2019**, *3* (8), 1426–1437.

(48) Wang, Y.; Piletic, I. R.; Takeuchi, M.; Xu, T.; France, S.; Ng, N. L. Synthesis and hydrolysis of atmospherically relevant monoterpene-derived organic nitrates. *Environ. Sci. Technol.* **2021**, *55* (21), 14595–14606.

(49) Wesely, M.; Hicks, B. Some factors that affect the deposition rates of sulfur dioxide and similar gases on vegetation. *Journal of the Air Pollution Control Association* **1977**, *27* (11), 1110–1116.

(50) Jensen, N.; Hummelshøj, P. Derivation of canopy resistance for water vapour fluxes over a spruce forest, using a new technique for the viscous sublayer resistance. *Agricultural and Forest Meteorology* **1995**, *73* (3-4), 339–352.

(51) Hall, B.; Claiborn, C.; Baldocchi, D. Measurement and modeling of the dry deposition of peroxides. *Atmospheric Environment* **1999**, *33* (4), 577–589.

(52) Rivera Rios, J. C. *Atmospheric chemistry of isoprene hydroxyhydroperoxides*; Harvard University: 2018.

(53) Tsiligiannis, E.; Wu, R.; Lee, B. H.; Salvador, C. M.; Priestley, M.; Carlsson, P. T.; Kang, S.; Novelli, A.; Vereecken, L.; Fuchs, H.; et al. A four carbon organonitrate as a significant product of secondary isoprene chemistry. *Geophysical Research Letters* **2022**, *49* (11), No. e2021GL097366.

(54) Place, B. K.; Delaria, E. R.; Cohen, R. C. Leaf Stomatal Uptake of Alkyl Nitrates. *Environmental Science & Technology Letters* **2022**, *9* (2), 186–190.

(55) Singh, H.; Salas, L.; Chatfield, R.; Czech, E.; Fried, A.; Walega, J.; Evans, M.; Field, B.; Jacob, D.; Blake, D. Analysis of the atmospheric distribution, sources, and sinks of oxygenated volatile organic chemicals based on measurements over the Pacific during TRACE-P. *Journal of Geophysical Research: Atmospheres* **2004**, *109* (D15), D15S07.